Journal of Molecular Catalysis A: Chemical 315 (2010) 171–177

Contents lists available at ScienceDirect

Journal of Molecular Catalysis A: Chemical

journal homepage: www.elsevier.com/locate/molcata

# The influence of Mg on the C adsorption on Ni(1 0 0): A DFT study

Hernán Milberg[a], Alfredo Juan[b], Norma Amadeo[a], Beatriz Irigoyen[a,*]

[a] Departamento de Ingeniería Química, Laboratorio de Procesos Catalíticos, Facultad de Ingeniería, Universidad de Buenos Aires, Ciudad Universitaria, 1428, Ciudad Autónoma de Buenos Aires, Argentina
[b] Departamento de Física, Universidad Nacional de Sur, Avda. Alem 1853, 8000, Bahía Blanca, Argentina

ARTICLE INFO

*Article history:*
Received 24 July 2009
Received in revised form
13 September 2009
Accepted 14 September 2009
Available online 22 September 2009

*Keywords:*
Mg promoter effect
Carbon deposition
Ni-based catalysts
DFT calculations

ABSTRACT

In this work, we performed density functional theory (DFT) calculations to study carbon adsorption on the Ni(1 0 0) surface and absorption in the bulk of nickel-based catalysts. The ideal catalyst surface was modeled as a five-layer Ni(1 0 0) slab. We also studied the influence of magnesium, considered as an atomic substitutional impurity, on carbon adsorption and migration into the bulk.

To study the effect of Mg on the structure of Ni-based catalysts, we replaced a Ni atom by a Mg atom, on the surface and also in the bulk. Then, we relaxed the Mg and Ni positions. Our results showed that Ni atoms were pushed away from Mg. We also performed energy calculations to evaluate carbon interactions on different preferential sites of the Ni-slab, and also the effect of Mg atom on these deposition processes.

The calculations showed that carbon adsorption on the bare Ni(1 0 0) surface was more favorable than deposition on this surface doped with magnesium. Our results also indicated that Mg could improve the interaction of surface-adsorbed carbon with gas phase oxygen, leading to the formation of a CO precursor species. In this way, magnesium promotes Ni-based catalysts hindering the surface from attaining a high carbon coverage, and thus making difficult the formation of carbon agglomerates and carbon whiskers. We also considered the effect of Ca in the C–O interaction on the metal surface.



## 1. Introduction

Syntheses gas (syngas), a mixture of hydrogen and carbon monoxide, is one of the most important feedstock for chemical syntheses and for the production of clean liquid fuels. Syngas is used in the production of ammonia, oxochemicals, and fuels (methanol, methanol to gasoline and to olefins), and in gas-to-liquids via Fischer–Tropsch processes upgrade [1–4]. Furthermore, syngas is predicted to play a key role in the hydrogen economy. Because of the disadvantages of hydrocarbon thermal power generation, low energy efficiency and environmental pollution, many researchers have focused their attention in devices able to convert chemical energy of the hydrocarbons directly into electric energy. These devices, highly efficient for producing electric energy by electrochemical oxidation of hydrogen on the anode, may considerably increase the demand for hydrogen in the near future.

The most important processes for the production of hydrogen and syngas are steam reforming (SR) of hydrocarbons and alcohols, partial oxidation (POX) and autothermic reforming (ATR) of hydrocarbons, and $CO_2$ reforming of methane [5–7]. Steam reforming (SR) provides a higher $H_2$/CO ratio (>3) feedstocks than that needed for Fischer–Tropsch synthesis and the production of methanol. In spite of this, SR combined with partial oxidation process (the so called autothermal reforming) produces syngas of more suitable stoichiometric $H_2$/CO ratio (∼2) for the methanol and Fischer–Tropsch synthesis [8]. However, in SR reactions, an excess superheated steam (S/C ∼ 2–3) in the feed gases is needed in order to inhibit carbon deposition on catalysts surface [9,10]. In autothermal reforming, the low steam to carbon ratio and high exit temperature reaction conditions favor the formation of coke. In order to obtain fuel cell quality hydrogen, the reforming step is generally followed by the CO abatement through water gas shift (WGS) and preferential oxidation (PROX) reactions. The addition of steam is usually required to push the WGS reaction, and hence C deposition is a less serious issue. Furthermore, in autothermal reforming, partial oxidation, and catalytic partial oxidation systems, additional constraints are imposed to C removal because the O/C ratio cannot be increased due to complete oxidation. Depending of the process it is often considered more important to have continuous C removal by $H_2O$, rather than O (continuously or periodically fed). Besides, C deposition on catalysts surface is usually/potentially more severe in syngas production, because low steam to carbon ratios are sometimes targeted for cost reasons, as well as issues concerning the downstream technology.

The composition of catalysts usually employed in most of the above mentioned processes are based on nickel [11,12]. An important concern about Ni-based catalysts is the deposition of carbon

* Corresponding author.
*E-mail address:* beatriz@di.fcen.uba.ar (B. Irigoyen).

1381-1169/$ – see front matter © 2009 Elsevier B.V. All rights reserved.
doi:10.1016/j.molcata.2009.09.008

on their surfaces, which constitutes a highly undesired process because C atoms could agglomerate, form stable structures and lead to catalyst deactivation. Deposited carbon atoms can also diffuse into the bulk and finally accumulate. This process leads to the formation of carbon filaments with nickel particles, detached from the catalyst surface, on their tips. Although the catalyst remains active for hydrocarbon reforming reactions, these whiskers can grow during the hydrocarbon processing and block the reactor. Alternatively, Pt, Pd or Rh containing catalysts have shown better properties in stability, activity and less tendency to carbon deposition than Ni catalysts [12]. It has been found that the catalytic performance of these catalysts for SR reactions varies in the order of Pt > Pd > Rh > Ru, with Pt exhibiting high activity and selectivity toward hydrogen production, as well as long term stability at low temperatures [13].

In spite of the carbon deposition, Ni-based catalysts are usually preferred for syngas production due to their high activity, stability, selectivity and attractive cost. It has been reported that carbon deposition during methane oxidation reactions depends on the size of nickel crystallites [14]. Thus, reducing their size it was possible to prevent the Ni sintering process and so the formation of carbon deposits [15]. The size of Ni crystallites has been modified by the incorporation of promoters or adding metal or oxide promoters, which influence the interaction of carbon atoms with the catalysts surfaces [14,16]. The doping with boron favored the dispersion of Ni particles, and reduced the formation of carbon deposits during methane reforming reactions [17]. The addition of Cr to a $Ni/Al_2O_3$ catalyst formed a Cr–Ni alloy with smaller ensembles of nickel crystals, and reduced the amount of carbon deposited during methane partial oxidation [18]. The activity, selectivity and coke formation resistance in acetylene hydrogenation reactions have also been improved by adding Zn to a monometallic Ni catalyst [19]. Silica supported nickel catalysts promoted with Cu have shown higher activity compared to NiO–MgO systems [20]. The catalytic behavior of $Ni/Al_2O_3$ modified with La and Ag has been investigated in ethanol steam reforming reactions [21–23]. Similar effects have been found for La on $Ni/CeO_2$ [24]. Nickel-based catalysts supported on Mg, Ca and Sr modified $Al_2O_3$ have been prepared from layered double hydroxides, being Ca the modifier that showed lower amounts of carbon deposits [25,26].

The behavior of Ni/MgO, Ni/CaO and $Ni/CeO_2$ has been studied in methane oxidation reactions, reporting that the Ni/MgO catalyst was especially resistant to carbon deposition [9]. Also, solid NiO–MgO solution has been reported as resistant to carbon deposition [9,27]. The introduction of magnesium into the $Ni–MgO–Al_2O_3$ catalysts preparation mixture led to the formation of small nickel crystallites with stronger hydrocarbon adsorption sites [28]. In addition, carbon species weakly bonded to the catalyst surface were evidenced in methane decomposition reactions at low temperatures. $Ni/Al_2O_3$ catalysts modified by calcium and magnesium have shown enhancements on their stability and selectivity in hydrocarbon steam reforming reactions [29,30]. Carbon filaments have been observed over different nickel supported catalysts, including magnesia-containing supports, but Ni–Mg catalysts promoted the formation of thin carbon fibers [31]. $Ni/Al_2O_3$ catalysts, synthesized from lamellar double hydroxides (LDHs) precursors, have been reported as exhibiting Ni metal particles highly dispersed in aluminum structure [32]. The catalysts test with different Mg/Ni ratios in ethanol steam reforming reactions showed that Mg/Ni ratios higher than 0.1 decreased the amount of deposited carbon.

The role of step sites in many catalytic reactions on metal catalysts has been recently reviewed [33]. This review paper underlined the collaboration of modern characterization techniques (STEM, HREM and others) and density functional theory (DFT) calculations to give a more quantitative explanation of the impact of step sites on catalyst activity and side reactions such as carbon formation. Modified embedded atom method (MEAM) potentials have been employed to study the interactions between a carbon atom and a Ni nanoparticle [34]. The results showed that surface carbon atoms were more stable than those in the bulk and in sub-surface interstitial positions, and the single walled and double-walled carbon nanotubes would be more favorable to form on Ni nanoparticle catalyst. DFT calculations have been performed to study C atoms adsorption on the Ni(1 0 0) surface, and diffusion into the subsurface [35]. C atoms strongly bonded at the surface fourfold hollow sites. The Ni(1 0 0) surface was not reconstructed for a carbon coverage of 0.11 monolayer (ML). However, when the critical carbon coverage of about 0.5 ML was reached the surface reconstruction was promoted and thus, C could easily diffuse into the bulk. Boron influence in carbon deposition on Ni-based catalysts has also been theoretically studied by performing DFT calculations [36]. Boron atoms blocked the octahedral sites of Ni, and prevented the diffusion of carbon into the bulk. Thus, carbon atoms remained on the surface and could be more easily removed by oxidation reactions. Also, on the basis of first principles simulations, it has been proposed that boron enhances the stability of Ni catalysts by selectively blocking both the subsurface and the step sites [37]. The strong preference of B atoms for the subsurface octahedral sites promoted the reconstruction of the Ni(1 1 1) surface. This reconstruction lowered the methane activation energy barriers, and hence subsurface boron atoms did not reduce catalyst activity. Additives such as K, S and Au improved the tolerance of Ni-based catalysts to carbon deposition [38]. These additives could also modify the mechanisms of hydrocarbon reforming reactions, and thus the optimum catalyst should contain enough additive to block carbon deposition, without compromising faster reaction channels. Similar results have been obtained for supported Au–Ni bimetallic catalysts [39]. This effect was attributed to the deposition of Au atoms on edges and steps of the catalyst surface, which blocked the most active sites for carbon nucleation. DFT calculations have also shown that low tolerance of Ni catalysts to carbon deposition can be improved synthesizing Ni alloys with elements located on their surfaces and able to promote the oxidation of the coke [40]. The Ni–Sn alloy avoided the formation of C–C bonds and so carbon nucleation.

At the initial stages of syngas production processes, $CH_x$ fragments were mainly decomposed on the Ni(1 0 0) surface and then the generated C atoms adsorbed and migrated on this surface [41,42]. DFT calculations of C adsorption and diffusion on Ni surfaces of low index have shown that Ni(1 0 0) is the most favorable face for C adsorption [43].

The development of Ni-based solids to catalyze syngas production with high resistance to carbon deposition is an attractive challenge. Earth alkaline metals (Mg and Ca) are frequently added to Ni-based catalysts to improve their stability and tolerance to coking. However, there are still some open questions about Mg microscopic effects on carbon deposition and diffusion processes. Therefore, in this work we performed DFT energy calculations to study the modifications in the Ni(1 0 0) structure due to the presence of substitutional Mg impurities. We studied Mg–Ni interactions on different sites on the surface and in the subsurface. We evaluated Mg and Ca influence on carbon deposition and accumulation, and also on C atom interaction with gas phase oxygen.

## 2. Computational method

Density functional theory (DFT) energy calculations [44,45] were implemented with the Vienna Ab-Initio Simulation Package (VASP) code [46–48]. In the last years, the VASP code has gained great attention because of its efficient self-consistent total energy calculations for complex systems of big size, including transitions metals. This high efficiency was attained by the introduction of adequate exchange-correlation functional.

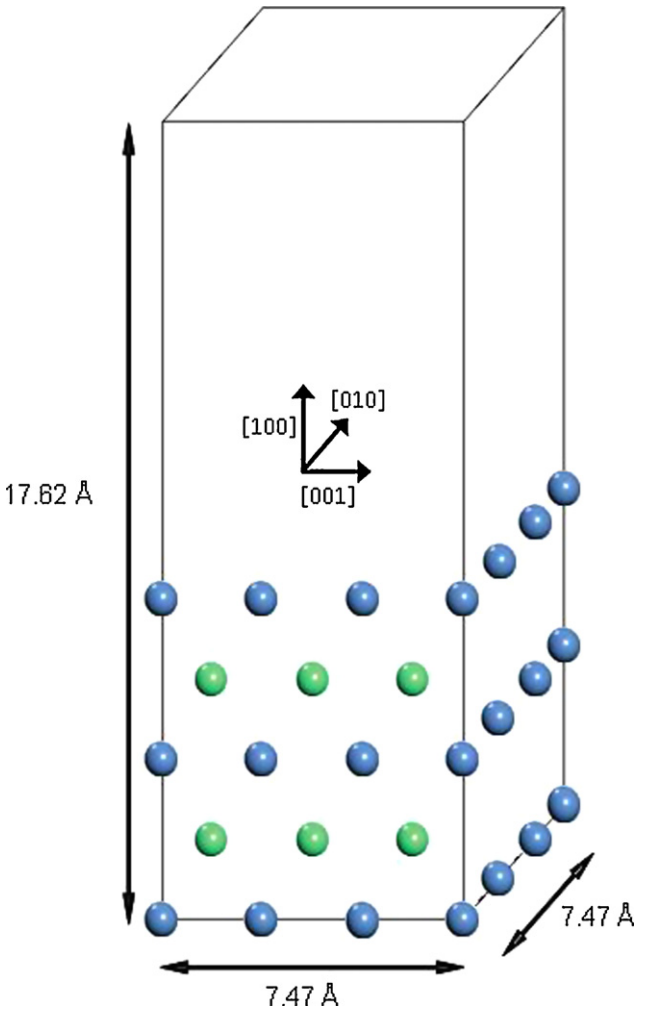


**Fig. 1.** Ni(1 0 0) supercell. Five-layers slab used for our DFT periodic calculations.

The Ni metal surface was modeled with the $Ni_{45}$(1 0 0) and $Ni_{44}Mg$(1 0 0) supercells. The Ni(1 0 0) surface was represented with a supercell formed by five-layers slab with 9 Ni atoms each, and a vacuum of about 11 Å in the vertical direction (see Fig. 1). This vacuum separated neighboring slabs, avoiding periodic interactions. We optimized the Ni atomic positions in the three upper layers of the slab, while Ni atoms of the two bottom layers were constrained to their crystal lattice geometry to mimic the bulk configuration. The interactions between valence electrons (Ni 4s, Ni 3d, C 2s and C 2p) and ion cores were represented by Bloch's all-electron-like projector augmented wave (PAW) method [49]. Exchange and correlation potentials of the Kohn–Sham theory were treated with the generalized gradient approximation (GGA) functional [50]. To calculate the electronic wave functions we employed plane wave basis set with an energy cutoff of 400 eV. The Brillouin zone was sampled with a Monkhorst–Pack grid [51], and electronic occupancies were determined according to a Methfessel–Paxton scheme [52]. For the ad(ab)-sorption energy calculations we considered spin polarization effects to represent the magnetic nature of Ni [53].

To model C–Ni interactions we employed three different systems: C–$Ni_{45}$(1 0 0), C–$Ni_{44}Mg$(1 0 0), and $Ni_{44}Ca$(1 0 0). In each case, the carbon adsorption energy ($\Delta E_{ads,C}$) was computed as the difference between the supercell total energy with one adsorbed C and the bare metal slab and C atom in vacuum:

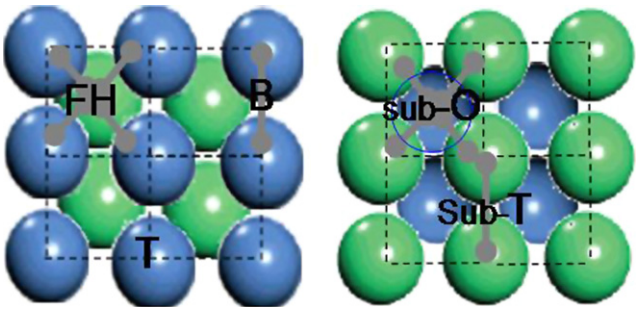


**Fig. 2.** Ni(1 0 0) structure. ( ) Surface Ni atoms. ( ) Second layer Ni atoms. Different sites for C–Ni interactions. FH: fourth hollow, B: bridge, T: top, sub-T: sub-tetrahedral and sub-O: sub-octahedral. (For interpretation of the references to color in this figure legend, the reader is referred to the web version of the article.)

(i) $\Delta E_{ads,C/Ni_{45}(100)} = E(C/Ni_{45}(100)) - E(Ni_{45}(100)) - E(C)$,
(ii) $\Delta E_{ads,C/Ni_{44}Mg(100)} = E(C/Ni_{44}Mg(100)) - E(Ni_{44}Mg(100)) - E(C)$,
(iii) $\Delta E_{ads,C/Ni_{44}Ca(100)} = E(C/Ni_{44}Ca(100)) - E(Ni_{44}Ca(100)) - E(C)$.

The energy corresponding to the C atom in vacuum was computed using a cubic box of 10 Å side, and including spin polarization.

Carbon atoms could interact with five different sites of the Ni(1 0 0) structure, which are shown in Fig. 2. Three of these sites are localized on the surface: the fourfold (FH), the top (T) and the bridge (B); and two in the subsurface: the bulk octahedral (sub-O), and the thetrahedral (sub-T) holes. The precision of PAW-GGA calculations for C adsorption on Ni(1 0 0) has been evaluated by comparing the calculated structural parameters to experimental observations of C bonding to hollow sites [35]. The authors found that the adsorption structure of C on Ni(1 0 0) at low coverages was correctly predicted. The calculated adsorption energies indicated the fourfold Hollow site as the most stable binding site for C adsorption in agreement with published experimental and theoretical studies [43,54]. In the subsurface, C atoms preferred the sub-O site which was about 1.20 eV lower in adsorption energy than the Hollow site. C adsorption on Ni(1 0 0) has also been experimentally studied through scanning tunneling microscopy (STM) [55]. The results indicated that at coverages less than 0.2 monolayer, C atoms were located at the fourfold hollow sites. Therefore, in this work we studied the interactions of carbon in the most stable Ni(1 0 0) (ad)absorption sites: the surface fourfold hollow (FH), and the subsurface octahedral (sub-O).

We evaluated the geometric distortions resulting from the introduction of Mg (Ca) impurity, by replacing a Ni atom for Mg (Ca) atom in the $Ni_{45}$(1 0 0) catalyst structure. Besides, we calculated the energy value for carbon interactions on the FH and in the sub-O sites of clean $Ni_{45}$(1 0 0), and $Ni_{44}Mg$(1 0 0) and $Ni_{44}Ca$(1 0 0) doped structures. Finally, we studied the interaction of the carbon deposited on these Ni(1 0 0)-based surfaces with gas phase oxygen. Carbon oxidation is an easy way to remove the coke from the catalyst, and hence we evaluated the influence of magnesium and calcium on this process.

## 3. Results

### 3.1. Ni(1 0 0)

We performed carbon energy ad(ab)-sorption calculations for the most favorable Ni(1 0 0) sites: the fourfold hollow (FH) on the surface, and the subsurface octahedral hole (sub-O).

In the case of $Ni_{45}$(1 0 0), the adsorption of carbon on a FH site did not modify the geometric position of the surrounding Ni atoms on this terrace. However, the four Ni atoms surround-

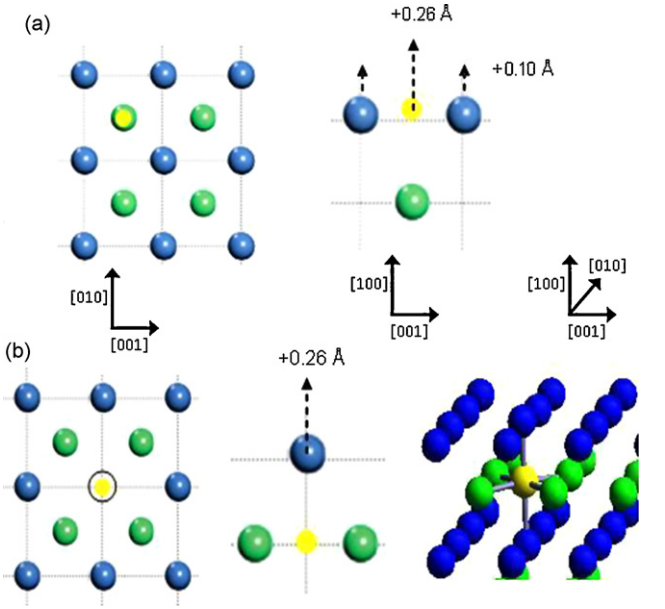


**Fig. 3.** (a) C atom deposition on a FH site of the $Ni_{45}(1\,0\,0)$ surface, and side view showing the movements of the surrounding Ni atoms. The small yellow circle represents the C atom. (b) C atom absorption in a sub-O site of the $Ni_{45}(1\,0\,0)$ structure, side and 3D views showing the movement of the Ni atom located over the C. The small yellow circle represents the C atom. In the left insert, the open circle represents the Ni atom above the C. (For interpretation of the references to color in this figure legend, the reader is referred to the web version of the article.)

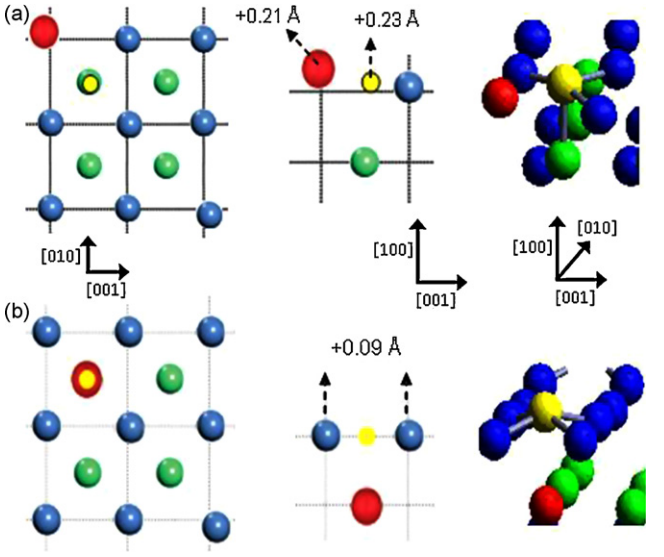


**Fig. 4.** (a) C atom deposition on a FH site of the $Ni_{44}Mg(1\,0\,0)$ surface, side and 3D views showing the movements of Mg (located on the surface) and C atoms. The small yellow circle represents the C atom. The big red circle represents the Mg atom. (b) C atom deposition on a FH site of the $Ni_{44}Mg(1\,0\,0)$ surface, side and 3D views showing the movements of Mg (located in the second layer) and C atoms. The small yellow circle represents the C atom. The big red circle represents the Mg atom. (For interpretation of the references to color in this figure legend, the reader is referred to the web version of the article.)

ing the carbon increased their vertical position in 0.1 Å. The C atom ended 0.26 Å above the surface, bonded with four surface Ni atoms (see Fig. 3a). The carbon formed four strong bonds with surface Ni atoms, and the value for the C atom adsorption energy was $\Delta E_{ads,C/Ni_{45}(100)} = -8.35$ eV. The carbon to nickel ratio of 1/9, represented a low coverage of 0.11 carbon monolayer. The Ni atoms located in the second and third metal layers did not show any significant displacements. We also studied the interaction of a carbon atom in the sub-O site, computing a value for the C absorption energy of $\Delta E_{abs,C/Ni_{45}(100)} = -7.12$ eV. The presence of carbon also modified the vertical coordinate of the surface Ni atom, located just above the carbon atom, which moved 0.26 Å outwards the surface (see Fig. 3b). Our calculated carbon ad(ab)-sorption energy values showed that C interaction in a sub-O site was 1.23 eV less favorable than on a FH site (see Table 1), in good agreement with the values previously reported in the literature [35].

### 3.2. $Ni_{44}Mg(1\,0\,0)$

We explored the effect of Mg impurities on the Ni(1 0 0) structure by replacing one Ni atom of the first layer for magnesium. Then, the geometric positions of the Mg and Ni atoms located in the three upper layers of the cell were relaxed. The results showed that Mg moves 0.49 Å upward the $Ni_{44}Mg(1\,0\,0)$ surface.

Regarding the C atom adsorption on a FH site of this surface (see Fig. 4a, left), our calculations allowed us to infer that the interaction between C and Mg atoms was repulsive. Magnesium moved on the surface 0.21 Å, in a diagonal direction away from its original location (see Fig. 4a, center). Also, the Mg atom increased its distance to the surface by 0.1 Å. At the same time the carbon atom made a bonding interaction with the surrounding Ni atoms. The carbon atom moved 0.19 Å away from magnesium on the (1 0 0) plane, and 0.23 Å in the vertical direction upward the surface. Our calculations showed that adsorbed C atom on a FH site of that structure bonded to three surface Ni atoms and to one Ni atom of the second layer (see Fig. 4a, right). The C lost of bonding to one surface Ni on Mg substituted structure (C formed four strong bond on the $Ni_{45}(1\,0\,0)$ one) is reflected in a lower value of the adsorption energy $\Delta E_{ads,C/Ni_{44}Mg(100)} = -7.94$ eV (see Table 1).

We also performed energy calculations for carbon adsorption on the $Ni_{44}Mg(1\,0\,0)$ surface with the Mg positioned in the second layer of the cell (see Fig. 4b). In this case, C adsorption almost did not change the Mg atom location. The four Ni atoms, neighbor to the carbon, moved 0.09 Å upwards the surface. The value of the C adsorption energy was $\Delta E_{ads,C/Ni_{44}Mg(100)} = -8.60$ eV (see Table 1), showing that the presence of magnesium in the subsurface favored the deposition of carbon.

Finally, we studied the influence of Mg on the adsorption of several carbon atoms (see Fig. 5a and b). In these calculations, the new added C atom, prior C-atoms adsorbed on the Ni(1 0 0) surface and Ni atoms of the three upper layers of the supercell were allowed to fully relax. After adsorption of a second carbon (C2), the three Ni atoms surrounding the C2 were moved 0.15 Å above the surface (see Fig. 5a). The value of the energy for the deposition of the second carbon was $\Delta E_{ads,C2/Ni_{44}Mg(100)} = -7.92$ eV, showing a repulsive interaction between C and Mg atoms. This behavior was similar to that previously seen for the adsorption of only one C atom ($\Delta E_{ads,C/Ni_{44}Mg(100)} = -7.94$ eV). Besides, after

**Table 1**
Binding energy (in eV) of carbon on the surface and in the subsurface of the clean and doped with Mg and Ca Ni(1 0 0) surfaces.

| | FH site | Sub-O site |
|---|---|---|
| $\Delta E_{ad(ab)s,C/Ni_{45}(100)}$ | −8.35 | −7.12 |
| $\Delta E_{ad(ab)s,C/Ni_{44}Mg(100)}$ [a] | −7.94 | −7.00 |
| $\Delta E_{ad(ab)s,C/Ni_{44}Mg(100)}$ [b] | −8.60 | −6.14 |
| $\Delta E_{ad(ab)s,C/Ni_{44}Ca(100)}$ [c] | −8.05 | – |

[a] Mg was positioned in the first layer of the cell.
[b] Mg was positioned in the second layer of the cell.
[c] Ca was positioned in the first layer of the cell.

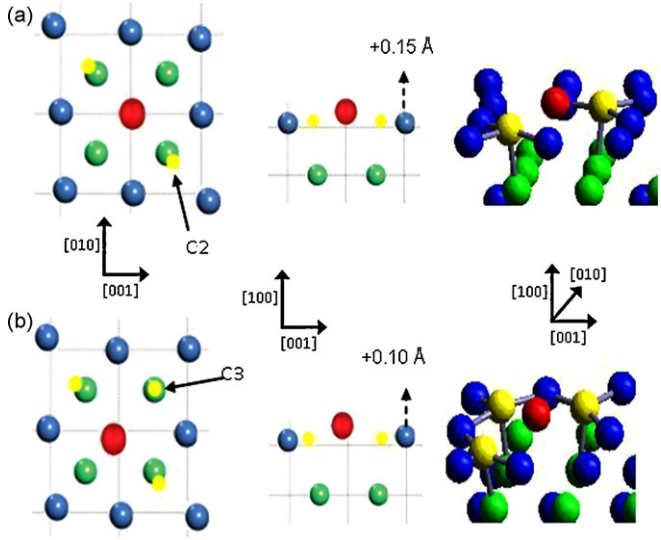


**Fig. 5.** (a) Adsorption of two C atoms on FH sites of the $Ni_{44}Mg(1\,0\,0)$ surface, side and 3D views showing the movements of the neighboring Ni atoms. The small yellow circle represents the C atom. The big red circle represents the Mg atom located on the surface. (b) Adsorption of three C atoms on FH sites of the $Ni_{44}Mg(1\,0\,0)$ surface, side and 3D views showing the movements of the neighboring Ni an Mg atoms. The small yellow circle represents the C atom. The big red circle represents the Mg atom located on the surface. (For interpretation of the references to color in this figure legend, the reader is referred to the web version of the article.)

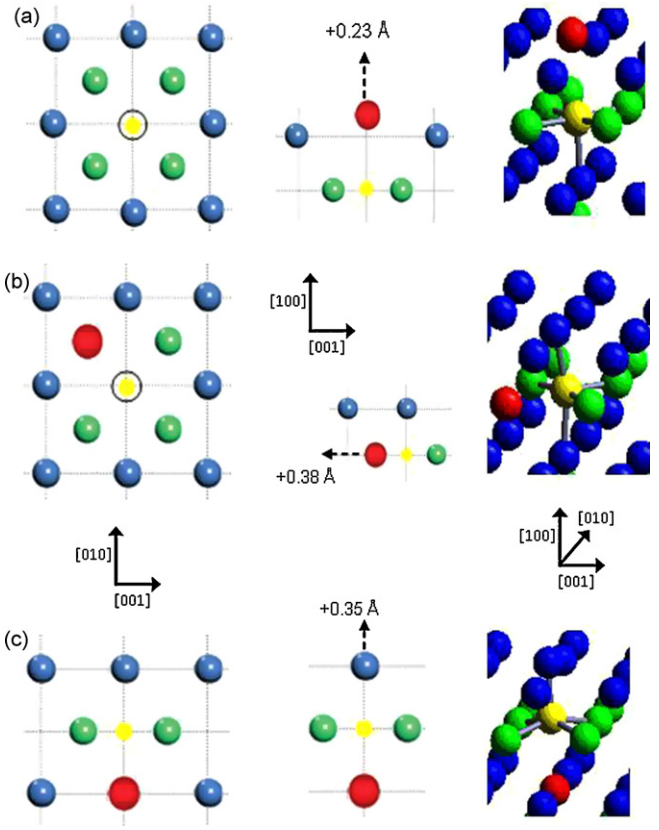


**Fig. 6.** (a) C atom deposition in a sub-O site of the $Ni_{44}Mg(1\,0\,0)$ structure, side and 3D views showing the movement of the Mg atom. The small yellow circle represents the C atom. The big red circle represents the Mg atom. In the left insert, the open circle represents the Mg atom on the surface, just above the C. (b) C atom deposition in a sub-O site of the $Ni_{44}Mg(1\,0\,0)$ structure, side and 3D views showing the movement of the Mg atom. The small yellow circle represents the C atom. The big red circle represents the Mg atom located in the second layer. In the left insert, the open circle represents the Ni atom above the C. (c) C atom deposition in a sub-O site of the $Ni_{44}Mg(1\,0\,0)$ structure, side and 3D views showing the movement of the Ni atom. The small yellow circle represents the C atom. The big red circle represents the Mg atom located in the third layer. (For interpretation of the references to color in this figure legend, the reader is referred to the web version of the article.)

adsorption of the third carbon (C3), the four Ni atoms surrounding C3 were pushed 0.10 Å above the surface (see Fig. 5b). The adsorption of the third carbon was more difficult than the previous ones, and the resulting energy value for this interaction was $\Delta E_{ads,C3/Ni_{44}Mg(100)} = -7.34\,eV$.

On the other hand, we studied C atom absorption in a sub-O site of $Ni_{44}Mg(1\,0\,0)$ structure. When the Mg atom was located just above the carbon, our calculations revealed that the C absorption energy value was similar to that in the structure without magnesium (see Table 1: $\Delta E_{ads,C/Ni_{44}Mg(100)} = -7.00\,eV$ vs. $\Delta E_{ads,C/Ni_{45}(100)} = -7.12\,eV$). Also, the C–Mg interaction was repulsive. The Mg vertical coordinate in this optimized geometry system was 0.23 Å higher than in the carbon free $Ni_{44}Mg(1\,0\,0)$ surface (see Fig. 6a). We also studied the influence of magnesium in the carbon absorption process when Mg was located in the second layer, just on side of the C atom. The calculations showed a C–Mg repulsive interaction, with Mg moving 0.38 Å away from carbon (see Fig. 6b). Moreover the C atom moved 0.25 Å upward, pushing the Ni atom located above it in the vertical direction. This process was the less favorable among all the studied in this work, as shown by the energy value for this carbon interaction listed in Table 1: $\Delta E_{abs,C/Ni_{44}Mg(100)} = -6.14\,eV$. Finally, we studied the absorption of C in the sub-O site of a catalyst with Mg replacing a Ni atom of the third layer, and located just below the carbon atom. The C–Mg interaction was repulsive and the C atom moved up in the vertical direction. The C-surface vertical distance was 0.36 Å longer than that observed in the Mg free structure. The Ni atom located above the carbon additionally increased its vertical coordinate in 0.35 Å, compared to its position on Mg free structure (see Fig. 6c). The energy value calculated for this process was $\Delta E_{abs,C/Ni_{44}Mg(100)} = -7.06\,eV$. Our calculations showed that the influence of Mg on C interactions on the surface and in the subsurface of Ni-based catalyst, was important only when magnesium occupied a position close to carbon, and in the same layer where C was deposited.

### 3.3. $Ni_{44}Ca(1\,0\,0)$

Taking into account the results available in the literature, referred to the promoter effect of calcium in the oxidation of the coke deposited on Ni-based catalysts, we also analyzed the adsorption of carbon on $Ni_{44}Ca(1\,0\,0)$ surface. We replaced a Ni atom of the surface by a Ca atom, in a similar way that we did in the case of Mg impurity (see Fig. 4a, left). Then, we relaxed the atomic geometric positions in the resulting structure. Our calculations showed that Ca atom is pushed 1.03 Å above the Ni surface.

When a C atom was adsorbed on a FH site of the $Ni_{44}Ca(1\,0\,0)$ surface, the carbon experienced a repulsive interaction with the alkaline element. On the surface, calcium moved away from carbon in a diagonal direction, ending at 0.33 Å from its original position. Calcium vertical coordinate also increased in 0.19 Å. The C atom located 0.17 Å upwards the surface. The resulting C adsorption energy value was $\Delta E_{ads,C/Ni_{44}Ca(100)} = -8.05\,eV$. Our findings, summarized in Table 1, showed that magnesium as well as calcium, disfavored the deposition of coke on Ni-based catalysts surface: $\Delta E_{ads,C/Ni_{44}Mg(100)} = -7.94\,eV < \Delta E_{ads,C/Ni_{44}Ca(100)} = -8.05\,eV < \Delta E_{ads,C/Ni_{45}(100)} = -8.35\,eV$.

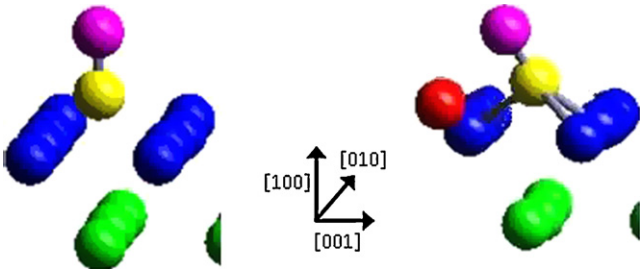


**Fig. 7.** CO precursor species formed on the (1 0 0) surface of Ni-based catalysts. Left: $Ni_{45}$(1 0 0), Right: $Ni_{44}Mg$(100). The small yellow and purple circles represent the C and O atoms, respectively. The big red circle represents the Mg atom located on the surface. (For interpretation of the references to color in this figure legend, the reader is referred to the web version of the article.)

### 3.4. Carbon oxidation

In this section we studied the reaction of the carbon adsorbed on Ni(1 0 0)-based catalysts with oxygen coming from the gas phase. We calculated the energy needed to form the CO species on the Ni(1 0 0) surface and also on those with Mg and Ca substitutional impurities. The rapid oxidation of the adsorbed C atoms would keep the Ni surface with a low carbon coverage, preventing the reconstruction of the Ni(1 0 0) surface and the C diffusion into the bulk.

The formation energy of the CO species on the different surfaces was computed as:

(iv) $\Delta E_{CO/Ni_{45}(100)} = E(CO/Ni_{45}(100)) - E(C/Ni_{45}(100)) - E((1/2)O_2)$,

(v) $\Delta E_{CO/Ni_{44}Mg(100)} = E(CO/Ni_{44}Mg(100)) - E(C/Ni_{44}Mg(100)) - E((1/2)O_2)$,

(vi) $\Delta E_{CO/Ni_{44}Ca(100)} = E(CO/Ni_{44}Ca(100)) - E(C/Ni_{44}Ca(100)) - E((1/2)O_2)$.

We estimated the C–O bond length for the CO molecule in vacuum by putting C and O atoms in a cubic box of 12 Å sides. The calculated C–O bond length for the spin-polarized calculation is 1.14 Å.

The approximation of oxygen to the C atom adsorbed on the $Ni_{45}$(1 0 0) surface, resulted in a C–O bonding interaction (C–O distance = 1.20 Å, see Fig. 7, left). This interaction also weakened the C–Ni bonds. The C atom was displaced from the Ni surface and moved 1.06 Å above it (see Table 2). At the same time, the Ni atoms descended 0.10 Å. The energy value calculated for the CO precursor formation process was $\Delta E_{CO/Ni_{45}(100)} = -2.26$ eV. When oxygen approached the carbon deposited in a Mg substituted Ni(1 0 0) surface, it experienced a bonding interaction with the C atom (C–O distance = 1.26 Å, see Fig. 7 right). The C atom moved 0.94 Å above the catalyst surface. The energy value calculated for the formation of the CO precursor was $\Delta E_{CO/Ni_{44}Mg(100)} = -2.77$ eV (see Table 2). The carbon oxidation process was similar on the Ca substituted Ni(1 0 0) surface. The C–O distance was 1.32 Å, with the C atom located 0.96 Å above the surface. The energy of this process was $\Delta E_{CO/Ni_{44}Ca(100)} = -2.80$ eV. These results, summarized in Table 2, showed that the formation of a CO intermediate species was more favorable on the Ca and Mg substituted Ni(1 0 0) surfaces. The desorption of the CO molecule from the different studied surfaces was an endothermic process. The energy required for the CO desorption from the Ni(1 0 0) surface was 1.93 eV, from the $Ni_{44}Mg$(1 0 0) is 2.03 eV, and from $Ni_{44}Ca$(1 0 0) is 2.18 eV, respectively.

**Table 2**
Formation energy and geometric parameters of the CO species on the Ni(1 0 0) clean and doped with Mg and Ca surfaces.

| | $\Delta E_{CO}$ (eV) | C–O distance (Å) | C–Ni distance (Å) |
|---|---|---|---|
| $Ni_{45}$(1 0 0) | −2.26 | 1.20 | 1.06 |
| $Ni_{44}Mg$(1 0 0) | −2.77 | 1.26 | 0.94 |
| $Ni_{44}Ca$(1 0 0) | −2.80 | 1.32 | 0.96 |

## 4. Discussion

Our DFT calculations showed that Mg modifies locally the surface structure of Ni catalysts, with the Ni atoms being pushed away from magnesium. This microscopic behavior could be interpreted as one of the basic characteristics of Mg promoter effect, the enhancement of small Ni aggregates formation. The calculations also confirmed that C atoms adsorbed preferentially on Ni surface, and that Mg disfavored the accumulation of carbon. This fact was true only when Mg was located near to the deposited C atom. When a Ni atom was substituted by Mg in the second layer, the energy of carbon absorption in the sub-O site decreased to −6.14 eV. This energy value was almost 1 eV lower than the calculated for a similar case with Mg located on the first layer. We also studied subsequent depositions of several C atoms. From these calculations, we could see that Mg made the C adsorption in any coplanar situation unfavorable. Thus, co-planarity of Mg with C would disfavor the formation of carbon deposits of big size. According to our calculations, a substitutional Mg did not avoid Ni(1 0 0) surface reconstruction. However, the Mg impurity seemed to be detrimental for the critical C coverage needed for that reconstruction. Both Mg and Ca impurities decreased the adsorption energy for carbon.

The interaction of oxygen with the preadsorbed C atom provided some indications for the formation of the CO precursor. Mg and Ca impurities favored the formation of this CO species. Note that, the C atom was moved away from the surface by this interaction. This process was more favorable when the Ni surface had alkaline substitutional impurities compared with the Ni clean surface. The C–O interaction also decreased the strength of C–Ni bonds. The calculations indicated that Ni-based catalysts could be promoted by adding Mg or Ca, which facilitated the oxidation of the adsorbed carbon species.

Our theoretical results were in good agreement with those obtained in our laboratory for ethanol steam-reforming reactions over Ni–Mg–Al-based catalyst [32]. The experimental tests were performed under favorable conditions for carbon deposition, and with different Mg/Ni ratios. The measurements showed that the amount of coke decreased up to 25% (w/w), for Mg/Ni ratios higher than 0.10. Hence, from both theoretical and experimental results we could connect the improvement of the performance of Ni-based catalyst to the Mg content. Magnesium could act not only as a neutralizer of the acidic sites of the support [56], but also as a Ni-based catalysts promoter which leaded to the formation of easily oxidizable carbon species.

## 5. Conclusions

Our calculations showed that Mg substitutional impurities modify locally the structure of the Ni-based catalysts, with the Ni atoms being pushed away from magnesium. In this way, the addition of Mg promoter leads to smaller Ni assembles. The deposition of carbon on Ni depends on the activation and decomposition of hydrocarbons, carbohydrates or CO, with several activation energies included, although our model did not consider the source of carbon, it was useful to understand the initial steps when the impurity was just on the surface. Carbon was preferentially adsorbed on the Ni surface. However, the presence of Mg as substitutional impurity interfered the deposition of C. Thus, Mg can prevent the formation of coke deposits of big size. In this way, magnesium also hinders the attaining of the critical carbon coverage needed for the

reconstruction of the Ni(1 0 0) surface, and hence makes difficult the diffusion of C atoms into the bulk and subsequent formation of whiskers.

Magnesium, as well as Ca, facilitated the interaction of gas phase oxygen with the adsorbed carbon promoting the formation of a CO precursor species.

## Acknowledgements

We specially thank H. Andrés Lagar-Cavilla for his help with setting up and optimizing our computing infrastructure. We also thank Universidad de Buenos Aires, Universidad Nacional del Sur, CONICET and ANPCyT-PICT 560/2007 for their financial support.

## References

[1] P. Howard, G. Morris, G. Sunley, in: G.P. Chiusoli, P.M. Maitheis (Eds.), Metal-Catalysis in Industrial Organic Processes, Royal Soc. Chem., Cambridge, 1996, p. 1.
[2] M.A. Peña, J.P. Gomez, J.L. Garcia Fierro, Appl. Catal. A: Gen. 144 (1996) 7–57.
[3] J.R. RostrupNielsen, in: J.R. Anderson, M. Boudart (Eds.), Catalysis: Science and Technology, Springer-Verlag, New York, 1984, p. 1.
[4] M.E. Dry, in: J.R. Anderson, M. Boudart (Eds.), Catalysis: Science and Technology, Springer-Verlag, New York, 1984, p. 106.
[5] S.C. Tang, J.B. Claridge, M.L.H. Green, Catal. Today 23 (1995) 3–15.
[6] J. Comas, F. Mariño, M. Laborde, N. Amadeo, Chem. Eng. J. 98 (2004) 61–68.
[7] A. Heinezel, J. Roes, H. Brandt, J. Power Sources 145 (2005) 312–318.
[8] J.R. Rostrup-Nielsen, J. Sehested, J.K. Norskov, Adv. Catal. 47 (2002) 65–139.
[9] S. Tang, J. Lin, K.L. Tan, Catal. Lett. 51 (1998) 169–175.
[10] J.R. Rostrup-Nielsen, Catal. Today 18 (1993) 305–324.
[11] Z.L. Zang, X.E. Verykios, Catal. Today 21 (1994) 589–595.
[12] J.R. Rostrup-Nielsen, J.H.B. Hansen, J. Catal. 144 (1993) 38–49.
[13] A.C. Basagiannis, P. Panagiotopoulou, X.E. Verykios, Top. Catal. 51 (2008) 2–12.
[14] H.S. Bengaard, J.K. Norskov, J. Sehested, B.S. Clausen, L.P. Nielsen, A.M. Molenbroek, J.R. Rostrup-Nielsen, J. Catal. 209 (2002) 365–384.
[15] K. Christensen, D. Chen, R. Lodeng, A. Holmen, Appl. Catal. A: Gen. 314 (2006) 9–22.
[16] B. Enger, R. Lødeng, A. Holmen, Appl. Catal. A: Gen. 346 (2008) 1–27.
[17] L. Chen, Y. Lu, Q. Hong, J. Lin, F. Dautzenberg, Appl. Catal. A 292 (2005) 295–304.
[18] M. González, N. Nichio, B. Moraweck, G. Martin, Mater. Lett. 45 (2000) 15–18.
[19] J. Rodríguez, A. Marchi, A. Borona, A. Monzón, J. Catal. 171 (1997) 268–278.
[20] M. Ermakova, D.Yu. Ermakov, G. Kuvshinov, Appl. Catal. A 201 (2000) 61–70.
[21] J. Liberatori, R. Ribeiro, D. Zanchet, F. Noronha, J. Bueno, Appl. Catal. A: Gen. 327 (2007) 197–204.
[22] A. Fatsikostas, D. Kondarides, X. Verykios, Catal. Today 75 (2002) 145–155.
[23] Z. Xu, Y. Li, J. Zhang, L. Chang, R. Zhou, Z. Duan, Appl. Catal. A: Gen. 213 (2001) 65–71.
[24] T. Zhu, M. Flytzani-Stephanopoulos, Appl. Catal. A: Gen. 208 (2001) 403–417.
[25] H. Morioka, Y. Shimizu, M. Sukenobu, K. Ito, E. Tanabe, T. Shishido, K. Takehira, Appl. Catal. A: Gen. 215 (2001) 11–19.
[26] T. Shishido, M. Sukenobu, H. Morioka, M. Kondo, Y. Wang, K. Takaki, K. Takehira, Appl. Catal. A: Gen. 223 (2002) 35–42.
[27] V.R. Choudhary, A.S. Mamman, Fuel Process. Technol. 60 (1999) 203–211.
[28] W. Gac, A. Denis, T. Borowiecki, L. Kepinski, Appl. Catal. A: Gen. 357 (2009) 236–243.
[29] J. Lisboa, D. Santos, F. Passos, F. Noronha, Catal. Today 101 (2005) 15–21.
[30] Ch-M. Chen, J.-M. Jehng, Appl. Catal. A: Gen. 267 (2004) 103–110.
[31] Y. Echegoyen, I. Suelves, M. Lázaro, M. Sanjuán, R. Moliner, Appl. Catal. A: Gen. 333 (2007) 229–237.
[32] A.J. Vizcaíno, P. Arena, G. Baronetti, A. Carrero, J. Calles, M. Laborde, N. Amadeo, Int. J. Hydrogen Energy 33 (2008) 3489–3492.
[33] J. Rostrup-Nielsen, J.K. Nørskov, Top. Catal. 40 (2006) 45–48.
[34] W. Xiao, M.I. Baskes, K. Choc, Surf. Sci. 603 (2009) 1985–1998.
[35] Y.-A. Zhu, X.-G. Zhou, De Chen, W.-K. Yuan, J. Phys. Chem. C 111 (2007) 3447–3453.
[36] J. Xu, M. Saeys, J. Catal. 242 (2006) 217–226.
[37] J. Xu, M. Saeys, J. Phys. Chem. C 113 (2009) 4099–4106.
[38] H. Bengaard, J. Norskov, J. Sehested, B. Clausen, L. Nielsen, A. Molenbroek, J. Rostrup-Nielsen, J. Catal. 209 (2002) 365–384.
[39] Y.-H. Chin, D.L. King, H.-S. Roh, Y. Wang, S.M. Helad, J. Catal. 244 (2006) 153–162.
[40] E. Nikolla, J. Schwank, S. Linic, J. Catal. 250 (2007) 85–93.
[41] F. van Looij, J.W. Geus, Catal. Lett. 45 (1997) 209–213.
[42] H. Wise, J. McCarty, J. Oudar, in: H. Wise, J. Oudar (Eds.), Deactivation and Poisoning of Catalysts, Marcel Deker Inc., New York, 1985, p. 19.
[43] Q.-M. Zhang, J.C. Wells, X.G. Gong, Z. Zhang, Phys. Rev. B 69 (2004) 205413–205420.
[44] P. Hohenberg, W. Kohn, Phys. Rev. B 136 (1964) 864–871.
[45] W. Kohn, L.J. Sham, Phys. Rev. A 140 (1965) 1133–1138.
[46] G. Kresse, J. Hafner, Phys. Rev. B 48 (1993) 13115–13118.
[47] G. Kresse, J. Furthmüller, J. Comput. Mater. Sci. 6 (1996) 15–50.
[48] G. Kresse, J. Furthmüller, Phys. Rev. B 54 (1996) 11169–11186.
[49] P.E. Blöchl, Phys. Rev. B 50 (1994) 17953–17979.
[50] J.P. Perdew, J.P. Burke, M. Ernzerhof, Phys. Rev. Lett. 77 (1996) 3865–3868.
[51] H.J. Monkhorst, J.D. Pack, Phys. Rev. B 13 (1976) 5188–5192.
[52] M. Methfessel, A.T. Paxton, Phys. Rev. B 40 (1989) 3616–3621.
[53] G. Kresse, J. Hafner, Surf. Sci. 459 (2000) 287–302.
[54] L.C. Isett, J.M. Blakely, Surf. Sci. 58 (1976) 397–414.
[55] C. Klink, L. Olesen, F. Besenbacher, I. Stensgaard, E. Laegsgaard, N.D. Lang, Phys. Rev. Lett. 71 (1993) 4350–4353.
[56] F. Aupretre, C. Descorme, D. Duprez, D. Casanave, D. Uzio, J. Catal. 233 (2005) 464–477.